INTERNATIONAL JOURNAL OF AUTOMOTIVE AND MECHANICAL ENGINEERING (IJAME)
ISSN: 2229-8649 e-ISSN: 2180-1606
VOL. 20, ISSUE 1, 2023, 10231 – 10246
DOI: https://doi.org/10.15282/ijame.20.1.2023.06.0791

ORIGINAL ARTICLE

Mechanism of Cone Wedge Shape Based Electronic Wedge Brake: Model and Experimental Validation

S. I. Haris [1,2], F. Ahmad[1], H. Jamaluddin[3], M. H. Che Hasan[4], A. K. Mat Yamin[1]; and A. S. Phuman Singh[1]

[1]Faculty of Mechanical Engineering, Universiti Teknikal Malaysia Melaka (UTeM), 76100 Hang Tuah Jaya, Melaka, Malaysia
[2]Kolej Kemahiran Tinggi MARA Masjid Tanah, Km 1, Persiaran Paya Lebar, Ramuan China Besar, 78 300 Masjid Tanah, Melaka, Malaysia
[3]Faculty of Engineering and Information Technology, Southern University College, 81300 Johor, Malaysia
[4]Faculty of Engineering Technology Electric and Electronic, Universiti Teknikal Malaysia Melaka (UTeM), 76100 Hang Tuah Jaya, Melaka, Malaysia

ABSTRACT – This paper describes a new design of an electronic wedge brake (EWB) system called the Cone Wedge Shape Based Electronic Wedge Brake (CW-EWB). The CW-EWB brake is made up of two cone wedges, one female and one male, stacked on top of each other. The CW-EWB is powered by the linear movement of a roller screw caused by the rotation of an electric motor through the roller screw, which causes the lower wedge to move tangentially to the disc brake, creating braking torque as the wheel rotates. A dynamic model of the CW-EWB that creates braking torque was built in this study, utilising a physical parametric estimate method. A torque tracking controller based on the proportional integral derivative (PID) control scheme is presented to ensure the CW-EWB model performs properly. The resulting mathematical model and control method were then experimentally tested using a braking test rig outfitted with multiple sensors and input-output (IO) devices. The performance of the brake mechanism is analysed in terms of actuator voltage, current, wedge position, wheel speed, and brake torque. Consequently, comparisons are made between experimental outcomes and simulated model responses. There are comparable trends between simulation results and experimental data, with an acceptable level of error.

ARTICLE HISTORY
Received: 16th June 2022
Revised: 15th Feb 2023
Accepted: 02nd Mar 2023
Published: 30th Mar 2023

KEYWORDS
Electronic wedge brake;
Cone wedge mechanism;
Position tracking control;
Brake test rig

INTRODUCTION

As the world enters the latest Industrial Revolution (IR 4.0), vehicle technologies have seen significant advancements, resulting in a shifting landscape in how vehicles should be driven. More specifically, the shift is toward autonomous vehicles that can assess their surroundings and operate without requiring human interactions. Aside from the precision of vehicle position control in the Autonomous Vehicle (AV), the Autonomous Emergency Braking (AEB) system is one of the most important systems to ensure the safety of a vehicle and keep it under control, even in challenging and unforeseen operating conditions [1-2]. One of the pillars of the AEB system is the intelligent braking system (IBS), which requires a fast-response actuator to react quickly and effectively in emergency situations [1-4]. As a result, a new braking system called electronic wedge brake (EWB) has been developed as a unique solution to this need, as it is a pure electronically controlled braking system with the potential to enhance vehicle safety by reducing braking time and enabling the full integration of advanced control characteristics in an autonomous vehicle.

Despite recent successes in producing various designs of electronic wedge brake, more work is needed to improve their capability and usability in automotive applications. All of the studies on the EWB system revealed only minor improvements that were dependent on the system's ability to produce braking torque and had some limitations, particularly in terms of EWB design and characterisation. According to the EWB studies, the problem of wedge jamming at the abutment is still not completely solved. Despite the fact that numerous studies on the subject have revealed several improvements, little attention has been paid to the optimisation of the wedge angle profile. To address the jamming issue that occurred in the first design [6], an improvement was made by using two brushless DC motors to push and release the wedge mechanism during braking [7-8]. Even though the wedge jammed problem was solved practically, the structure became more complex than in the previous design. Moreover, the high cost and dependability of the double motors used must be considered.

In order to overcome the wedge jammed at the abutment and the disadvantage of using a double motor, researchers have since refocused their efforts on developing an EWB based on a single motor [1,9-35] by replacing the used actuator [13,15-17,36]. Several researchers have replaced the DC motor with a typically retracting solenoid actuator [16,33] and a variable force solenoid actuator [17] on the assumption that a greater pulling force is required to free the wedge from a jammed state. Aside from that, a number of researchers continue to use DC motors in the EWB design by incorporating additional features, such as a pushrod non-self-locking screw to activate push and release [10], a roller bearing as the abutment [9], and a worm gearing system to activate the wedge mechanism [22,29]. Based on the results of the conducted

*CORRESPONDING AUTHOR | Fauzi Ahmad | ✉ fauzi.ahmad@utem.edu.my

experiments, these extra features are very effective at preventing wedge mechanism jamming; consequently, they have become a common feature of the EWB design [19-21,23,28-30].

Despite the advantageous incorporation of extra elements into the EWB design, the study on the wedge angle profile received little consideration. Regardless of the forms of EWB, the majority continued to use the same wedge angle [3,7,8,12,14-19,21,24-27,29,30,33,34,37-39] without considering how to determine the optimal wedge angle to reduce the force necessary to pull the wedge out of the abutment. The only differences in design are likely the shape of the wedge and the arrangement of the wedge mechanism in the braking system, which are V-type [8], W-type [22], cross-type [10], and spiral-type wedge profiles [20]. Even so, the wedge angles in these mechanisms were not properly optimised. As a consequence, even if an improvement to the wedge profile is proposed, it will not solve the jamming problem. Moreover, the study and development of EWB, particularly with regard to wedge optimisation, is still restricted and represents an unexplored area of research.

In order to contribute to the advancement of EWB design, a new EWB-based cones wedge shape mechanism is proposed in this study. The design is divided into male and female mechanisms to ensure that the wedge can displace tangential to the brake rotor, preventing the wedge from sliding out of the track during braking. The actuator force angle generated in this design is to be the same as the wedge angle profile, with the expectation that the repulsive force and EWB brake efficiency will increase. A dynamic model of the EWB-based Physical Parametric Estimation Model, as well as a control strategy, have been developed based on the design. To demonstrate the validity of the proposed EWB's mathematical model, an experimental study was carried out using the EWB test rig and some braking procedures, as described in the following sections.

This paper is organised as follows: the first section includes an introduction and a review of some preliminary works on design and related work on EWB. The second section introduces the modelling design, working principle, and dynamic model of the proposed EWB system dynamic model. The third section describes the wheel dynamic modelling for EWB testing, followed by the inner and outer loop controls of the EWB actuator in section four. The prototype of the EWB is described in section five, in which all experimental issues, including test rig hardware and experimental setup, are described in detail. The sixth section focuses on the performance evaluation of the proposed EWB, and the final section provides the study's conclusion.

CONE WEDGE BASED ELECTRONIC WEDGE BRAKE (CW-EWB) MODELLING

Figure 1 depicts the CAD design of the wedge mechanism and the calliper of the CW-EWB from a variety of angles. The wedge mechanism consists of two wedge blocks that are shaped as half cones and are referred to as male and female. The male wedge shape is located at the lower wedge mechanism, and the female wedge shape is located at the upper wedge mechanism. The cone-shaped wedge mechanism is designed to ensure that the inner wedge moves in only one axis, which is in the *x*-direction rather than in both the *x* and *y* directions. The design was motivated by a problem that developed in our earlier design [3] when the wedge reached its maximum displacement and self-energised, causing the wedge to slip off the track in the lateral direction as the drive torque from the wheel retracted the lower wedge.

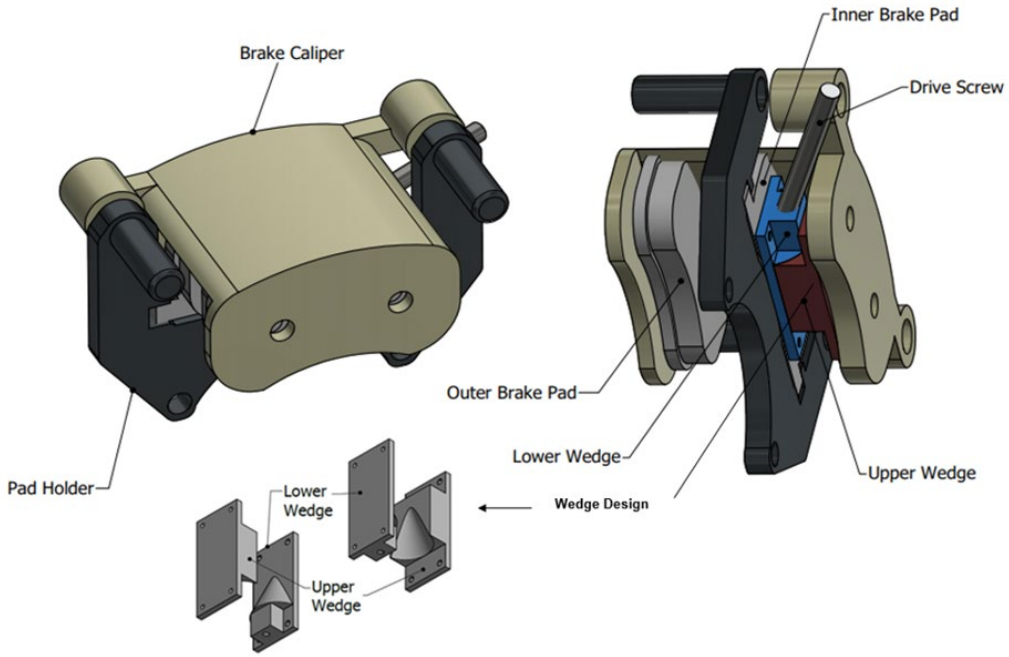

Figure 1. CW-EWB CAD design

CW-EWB Mechanism

Due to the fact that the effective braking force generated is dependent on the wedge angle, determining the optimal wedge angle is essential. Since the optimal wedge angle is interdependent on the friction coefficient of the brake pad, the brake pad should be chosen first. These two factors play a crucial role in the initial decision-making process in order to increase the braking force and prevent wedge sticking probability. As a result, in this study, the brake pad used in a Malaysian national car, as shown in Figure 2, was chosen for the EWB design consideration, particularly the wedge angle. According to the SAE standard on brake pads [40], the F code on the pad indicates that the coefficient of friction of the pad is between 0.35 and 0.45, as shown in Table 1.

Figure 2. Brake pads

Table 1. Friction coefficient coding [40]

Code letter	Coefficient of friction
C	Not over 0.15
D	Over 0.15 but not over 0.25
E	Over 0.25 but not over 0.35
F	Over 0.35 but not over 0.45
G	Over 0.45 but not over 0.55
H	Over 0.55
Z	Unclassified

Static Modelling of CW-EWB

The works of [3,6,28,41] were followed in order to select an appropriate wedge angle profile. Figure 3 depicts the body diagram of an EWB wedge mechanism, which is based on [12,42]. Note that α is the wedges angle, F_m is the motor force, F_c is the clamping force between the disc and the brake pad, F_b is the stopping force generated from the relative motion between the pad and the disc surface, and F_r is the wedge friction force that occurs between the upper and lower wedges. In this case, the angle of the driver screw β is set to be equal to α in order to amplify the force coming from the motor.

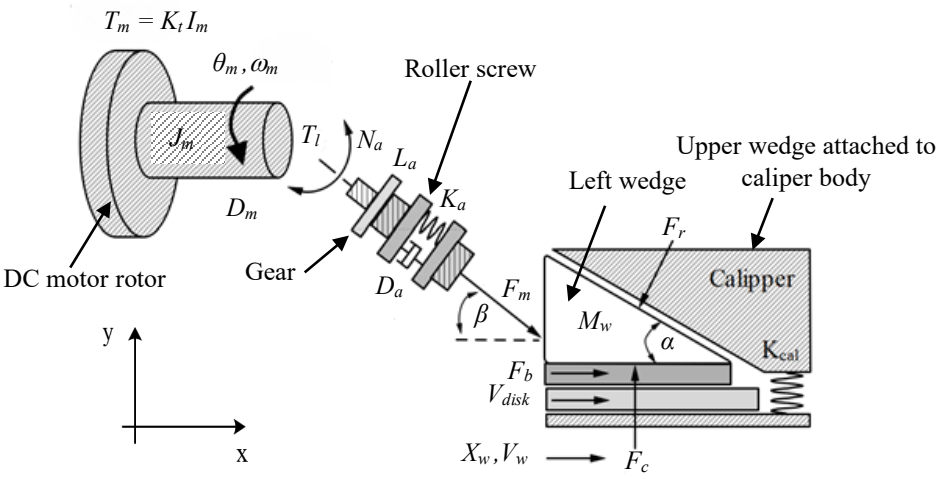

Figure 3. Basic body diagram of EWB

Assuming that the motor force is distributed equally on both sides of the wedges and the forces acting on the left wedge are the same as the one on the right, the relationship between the wedge pushing force, reaction force, clamping force and braking force on the disc for both sides of the wedges are derived as follow:

Summation of forces in the direction of *y*:

$$F_r \cos\alpha = F_c - F_m \sin\beta \tag{1}$$

Since,

$$F_b = \mu F_c \tag{2}$$

therefore,

$$F_r \cos\alpha = \frac{F_b}{\mu} - F_m \sin\beta \tag{3}$$

and summation of forces in *x* direction is:

$$F_r \sin\alpha = F_b + F_m \cos\beta \tag{4}$$

By dividing Eq. (4) with Eq. (3), the summation of force at the wedge can be defined as follows:

$$\frac{F_r \sin\alpha}{F_r \cos\alpha} = \frac{F_b + F_m \cos\beta}{\left[\frac{F_b - \mu F_m \sin\beta}{\mu}\right]} \tag{5}$$

therefore,

$$\tan\alpha = \frac{\mu(F_b + F_m \cos\beta)}{F_b - \mu F_m \sin\beta} \tag{6}$$

Rearrange the equations; the final equation of F_b to F_m is as follows:

$$F_b = F_m \left[\frac{\mu(\cos\beta + \sin\beta \tan\alpha)}{\tan\alpha - \mu}\right] \tag{7}$$

Since there is a pair of brake pads mounted on each wheel which creates a double brake force, the brake factor, C * is:

$$C^* = \frac{F_b}{F_m} = \left[\frac{2\mu}{\tan\alpha - \mu}\right](\cos\beta + \sin\beta \tan\alpha) \tag{8}$$

Equation (8) can be simplified to emphasise the additional feature produced by the wedge brake's specific actuation angle, where the new connection of the braking force to β and α can be explained as:

$$f(\beta, \alpha) = \cos\beta + \sin\beta \tan\alpha \tag{9}$$

thus, Eq. (9) can be derived as:

$$f(\beta, \alpha) = \cos\beta + \sin\beta \frac{\sin\alpha}{\cos\alpha} \tag{10}$$

The actuation angle (β) should be positioned at the same angle as the wedge angle (α) to ensure maximum amplification of the brake factor. Thus Eq. (10) can be simplified as follow:

$$f(\beta, \alpha) = \frac{\cos^2\beta + \sin^2\beta}{\cos\beta} \tag{11}$$

According to trigonometry formula,

$$\cos^2\beta + \sin^2\beta = 1 \tag{12}$$

and thus, the final equation for optimised EWB brake factor, C^* is simplified to be:

$$C^* = \frac{F_b}{F_m} = \frac{2\mu}{\tan\alpha - \mu}\left(\frac{1}{\cos\beta}\right) \tag{13}$$

where:

$$\beta = \begin{cases} 0, & \text{Current } EWB \\ \alpha, & \text{Optimise } EWB \end{cases} \tag{14}$$

Figure 4 depicts the effect of actuation angle on the characteristic brake factor, C^*.

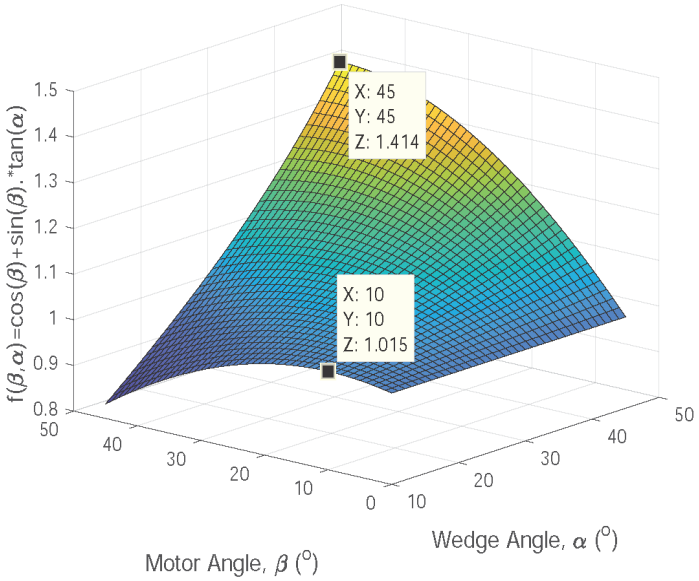

Figure 4. Effect of actuation angles and wedge angles towards EWB characteristic brake factor

The established wedge angle brake factor is monitored for the standard and optimum wedge brake, as shown in Figure 5. The self-reinforcement resulting from friction of the wedges to the disc brakes would be at the highest friction coefficient of 0.45, which is around 24.23 degrees, identical to tan $\alpha = \mu$, so no motor force is needed. Nonetheless, it is quite difficult to check the wedge position when this pad coefficient amount is raised because the brake factor is so great. While the brake force is strong, the wedge might become overly sensitive, even when the motor's power is minimal. However, if the pad coefficient is less than this value, it makes it difficult for the actuator to shift the wedge. When the pad and disc come into contact, the braking force generated is greater than the force generated by the actuator, and the wedge requires more pulling power to be released. Thereby, the optimum wedge angle of 24.5 degrees was selected based on the brake pad coefficient with optimisation to ensure that greater clamping forces can be generated and easily handled and the wedge is not jammed. Furthermore, the optimised EWB has a higher brake factor value than the standard EWB.

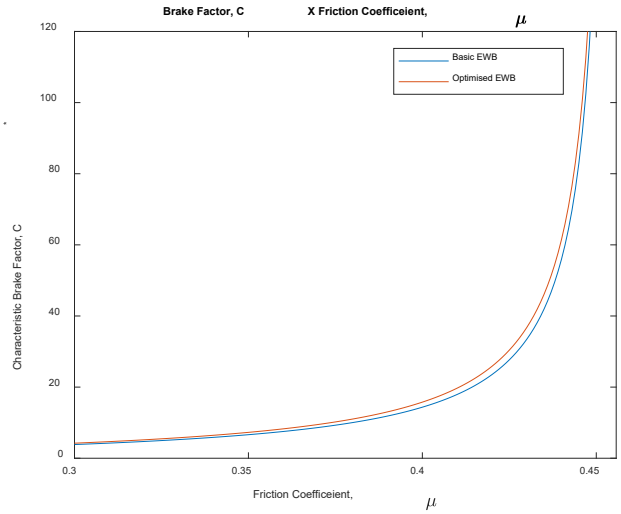

Figure 5. Characteristic brake factor, C* with a wedge angle of 24.5 degrees

The performance of the selected wedge angle can be evaluated by applying the required motor force and adjusting the coefficient of friction. Figure 6 was created by estimating a braking force of 7152 N and varying the coefficient of friction from 0.35 to 0.45. The figure shows that in the initial state, a 982.96 N of motor force is required to produce the necessary clamping force. Although the friction coefficient is 0.455, self-reinforcement occurs, and no motor force is required. As a consequence, the CW-EWB CAD design shown in Figure 1 was created using the optimised wedge angle.

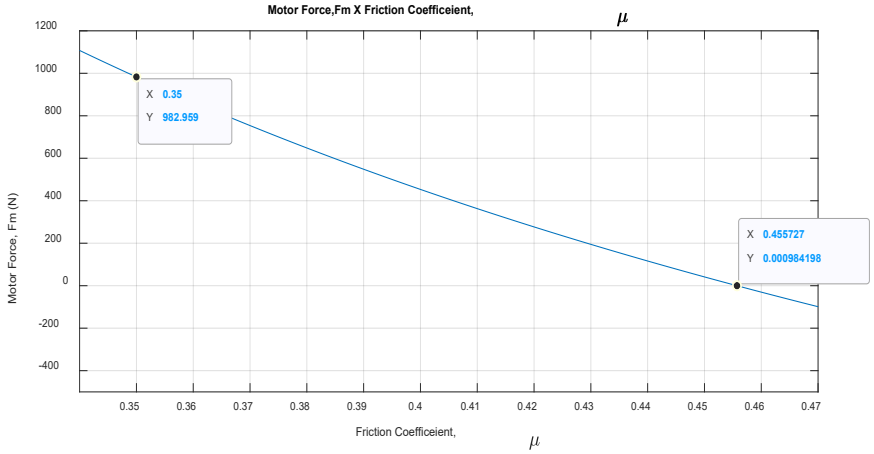

Figure 6. Motor force versus coefficient of friction

CW-EWB Dynamic Model

The actuator in this study was a permanent magnet direct current (PMDC) motor. Essentially, the PMDC motor is modelled by taking electrical and mechanical components into account. Here (J_m) is the inertia of the motor, (K_t) is the constant torque, (K_e) is the electromotive force constant, (D_m) is the viscous friction motor constant, and (T_l) is the load torque. Noting that (K_t) = (K_e) if there is no electromagnetic loss in the motor, the electrical power dissipated by the EMF back in the armature is directly converted to mechanical power.

The mathematical equations of the PMDC motor are shown as follows. For the armature circuits:

$$\dot{I}_m = -\frac{K_e}{L_m}\omega_m - \frac{R_m}{L_m}I_m + \frac{1}{L_m}V_m \tag{14}$$

By considering the mechanical load, the rotational acceleration of the DC motor shaft is described as:

$$\dot{\omega}_m = -\frac{D_m}{J_m}\omega_m + \frac{K_t}{J_m}I_m - \frac{1}{J_m}T_l \tag{15}$$

Here, a single lead screw-type start connects the PMDC motor directly to the brake mechanism. The required actuation force is then obtained by attaching the lead screw and a lossless planetary reduction gear to the heart mechanism.

Referring to Figure 2, the necessary motor drive force (F_m) can be calculated by considering several parameters of the lead screw, such as the steadiness of the lead screw (K_a), the viscous damping of lead screw (D_a), the reduction of the lead screw gear ratio, (N_a) and the screw lead, (L_a). The lead screw plays an important role in turning the engine angle (θ_m), engine speed (ω_m), and engine torque screw (T_{screw}) into wedge position (X_w), wedge speed (V_w), and motor force (F_m). Remember that when viewed from the motor side, the motor torque screw (T_{screw}) is an engine load (T_l).

The torque delivered to the screw can be represented by:

$$T_{screw} = \frac{N_a L_a}{2\pi\eta}\left[K_a\left(L_a\frac{N_a\theta_m}{2\pi} - \frac{X_w}{\cos\beta}\right) + D_a\left(L_a\frac{N_a\dot{\theta_m}}{2\pi} - \frac{V_w}{\cos\beta}\right)\right] \tag{16}$$

$$F_m = 2\pi\eta\frac{T_{screw}}{N_a L_a} \tag{17}$$

By substituting Eq. (16) into Eq. (17), the motor force (F_m) can be defined as:

$$F_m = K_a\left(L_a\frac{N_a\theta_m}{2\pi} - \frac{X_w}{\cos\beta}\right) + D_a\left(L_a\frac{N_a\dot{\theta_m}}{2\pi} - \frac{V_w}{\cos\beta}\right) \tag{18}$$

as Eq. (16), with the assumption that the planetary reduction gear mass is very light and the gear mechanism is less frictional. The lead screw output value ranges from 0 to 1. This is primarily determined by the geometry of the contact

surfaces, their finishing, and the lead screw thread is helix angle. It is also affected by operational factors such as load, speed, and lubrication. Although the efficiency of a lead screw is a true measured value, objective testing is the best way to determine the results. According to [43-45], the output of the lead screw used varies within a certain tolerance from its nominal value. As a result, the efficiency of the lead screw has been estimated to be 0.65 in this case.

Consider the EWB with the angle of the motor shaft, β, as in Figure 2. The relationship between the wedge actuation forces (F_m), reaction forces (F_r), and clamping forces (F_c) to the disc are derived based on force balance as follows: The dynamic of a wedge in the x-direction:

$$F_m \cos\beta + \mu F_c - F_r \sin\alpha = M_w \dot{V_w} \tag{19}$$

By dividing with tan α, yields,

$$F_r \cos\alpha = \frac{F_m \cos\beta + \mu F_c - M_w \dot{V_w}}{\tan\alpha} \tag{20}$$

Besides that, the dynamic of a wedge in the y-direction can be stated as follows:

$$F_m \sin\beta + F_r \cos\alpha - F_c = M_w \dot{V_w} \tan\alpha \tag{21}$$

Where M_w and V_w are wedge mass and wedge velocity in the x-direction, respectively, substituting Eq. (20) into Eq. (21), produces:

$$\dot{V_w} = \frac{F_n(\mu - \tan\alpha)}{M_w(\tan^2\alpha + 1)} + \frac{F_m(\sin\beta \tan\alpha + \cos\beta)}{M_w(\tan^2\alpha + 1)} \tag{22}$$

From Eq. (22), we want to simplify the complex multiplier formula of motor force (F_m), which is a function of the motor actuation angle and the wedge angle $f(\beta, \alpha)$. To maximise brake factor multiplication, the motor shaft angle should be the same as the wedge angle rather than a zero angle, as on a standard EWB. Assuming the two angles are equal, this function can be summarised as follows:

$$f(\beta, \alpha) = \cos\beta + \sin\beta \tan\beta \tag{23}$$

thus,

$$f(\beta, \alpha) = \frac{1}{\cos\beta} \tag{24}$$

Thus, the simplified wedge dynamic model can be described as:

$$\dot{V_w} = \frac{1}{M_w(\tan^2\alpha + 1)}\left[F_c(\mu - \tan\alpha) + \frac{F_m}{\cos\beta}\right] \tag{25}$$

Meanwhile, the clamping force depends on the calliper stiffness (K_{cal}), wedge displacement, and wedge angle given by:

$$F_c = K_{cal} X_w \tan\alpha \tag{26}$$

Substitute Eq. (26) into Eq. (25) produces:

$$\dot{V_w} = \left[\frac{K_{cal} \tan\alpha\,(\mu - \tan\alpha)}{M_w(\tan^2\alpha + 1)}\right] X_w + \left[\frac{1}{M_w(\tan^2\alpha + 1)\cos\beta}\right] F_m \tag{27}$$

The parameters used in the study are listed in Table 2.

Table 2. EWB DC carbon-brush motor model IG-420024X parameters

Parameter, Symbol	Value
Motor resistance, R_m	0.4781 Ω
Motor inductance, L_m	0.0230 H
Electromotive force constant, K_e	0.0158 N.m/A
Torque constant, K_t	0.0156 N.m/A
Motor moment inertia, J_m	7.094×10^{-3} Kg.m^2/s^2
Motor viscous friction constant, D_m	1.9175×10^{-5} N.m.s
Gear reduction, N_a	1/24
Axial stiffness, K_a	750×10^6 N/m
Axial viscous friction constant, D_a	9.3279×10^{-5}
Lead screw efficiency, η	0.63
Lead screw Pitch, L_a	3 mm
Wedge weight, M_w	0.3 Kg
Wedge angle, α	24.5 degree
Motor axial angle, β	24.5 degree
Calliper stiffness, K_{cal}	44.8385×10^6 N/m
Brake pad coefficient, μ	0.35

Wheel Dynamic Model for Simulation Testing of CW-EWB

In this study, the wheel dynamic model shown in Figure 7 is used to simulate and assess the performance of the CW-EWB. It is then used for system analysis, control law design, and computer simulations. Although the developed model is relatively simple, it retains the essential features of the actual system. As shown in Figure 6, it consists of a drive shaft that connects to the three-phase motor via belting to provide throttle torque, an MRB that provides brake torque, and a steel load that represents a dynamic wheel. The model defines the wheel speed as a state variable and the torque applied to the wheel as an input. The state equations are the result of applying Newton's law to wheel and vehicle dynamics. The dynamic equation for the angular motion of the wheel is as follows:

$$\tau_d - \tau_b = J_{all}\dot{\omega} \tag{28}$$

where, τ_b is the brake torque, τ_d is the drive torque while the shaft is rotating, $\dot{\omega}$ is the angular acceleration of the wheel and J_{all} is the total inertia which acts on the system. Since the rotation of the drive shaft is initiated by the motor torque (τ_m), and amplified by the load torque (τ_{load}) that has a mass (m) rotating within the effective radius (r), then τ_d can be rewritten as:

$$\tau_d = \tau_m + \tau_{load} + \tau_{wheel} \tag{29}$$

in which,

$$\tau_{load} = m_{load}\, g r_{load} \tag{30}$$

while

$$\tau_{wheel} = m_{wheel}\, g r_{wheel} \tag{31}$$

where m_{wheel} is mass of the wheel, m_{load} is mass of the wheel, while r_{load}, g is acceleration of gravity and r_{wheel} are the effective radius of load and wheel, respectively.

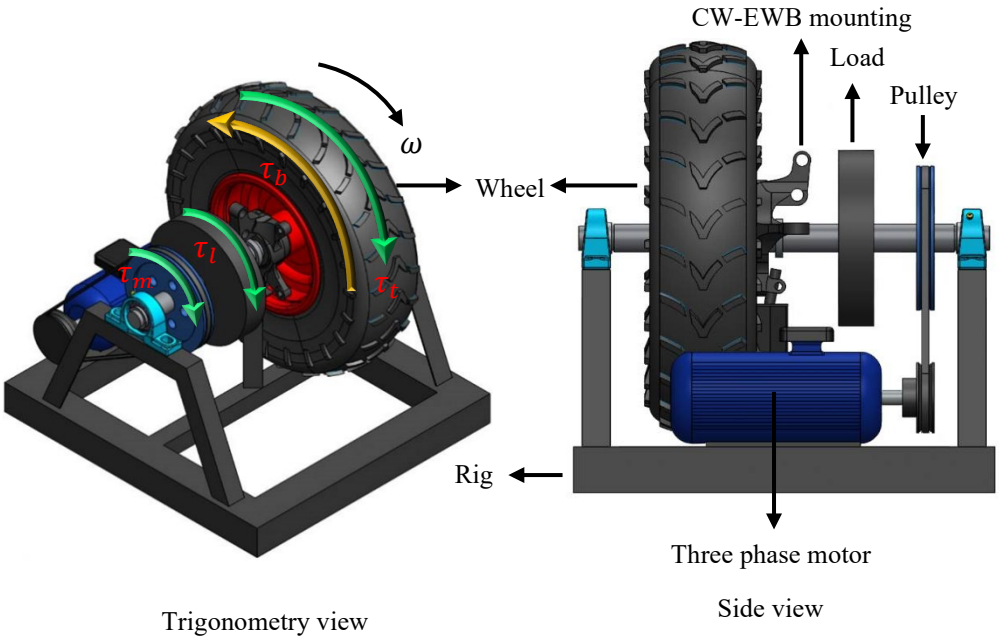

Figure 7. Wheel dynamic model

Figure 8 shows the clamping force and brake torque interface with the brake disc. By referring to the diagram, the braking torque, T_b, at the contact interface can be estimated as follows:

$$T_b = R_{eff} F_c \tag{32}$$

where R_{eff} is the pad's effective radius and F_c is the clamping force. However, at the contact interface, the friction force produced by F_b is dependent on the normal force (F_n) and friction coefficient (μ), which are defined as:

$$F_b = \mu F_n \tag{33}$$

The normal force strength is equal to the clamping force F_c on the top of the pad shown in Figure 8. Since the braking device has two brake pads, the total brake torque is:

$$T_b = 2R_{eff} \mu F_c \tag{34}$$

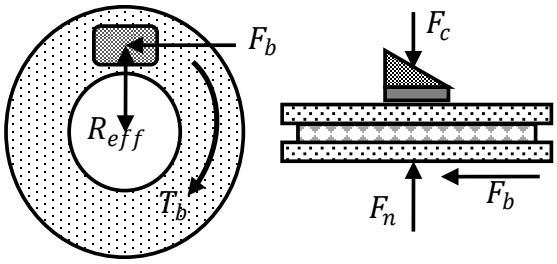

Figure 8. Brake torque model in contact interface, taken with permission from Ahmad et al. (2017), Journal of Mechanical Engineering, Copyright 2017 [3]

CW-EWB Control Structure

Designing a control scheme that determines the overall braking capability of the system is one of the most crucial aspects of EWB. As demonstrated by prior research [1,3-35], there are two techniques used for brake control; force- and torque-based control. In the majority of these studies, force control was favoured over torque control for controlling the EWB, as it is difficult to obtain torque feedback data measurements from the wheel. Due to the unavailability of a suitable force sensor to be mounted in the wedge mechanism, the torque control approach proposed by [1,3,4,38,45,46] was applied in this study. As shown in Figure 9, torque tracking control was implemented to the CW-EWB. As shown in the figure, it consists of two primary controller loops: torque control to regulate the overall output torque from the CW-EWB and position control to regulate the motor's position in order to track the desired torque. For the torque control loop, a proportional-integral-derivative (PID) controller was used to obtain the desired response and ensure that the desired braking torque was tracked accurately. While position control with the proportional-integral PI controller is utilised for

the DC motor to manage actuation, maintaining the desired spacing between the pad and the disc brake. Table 3 lists the parameters of the controllers that were tuned using the Ziegler-Nichols approach.

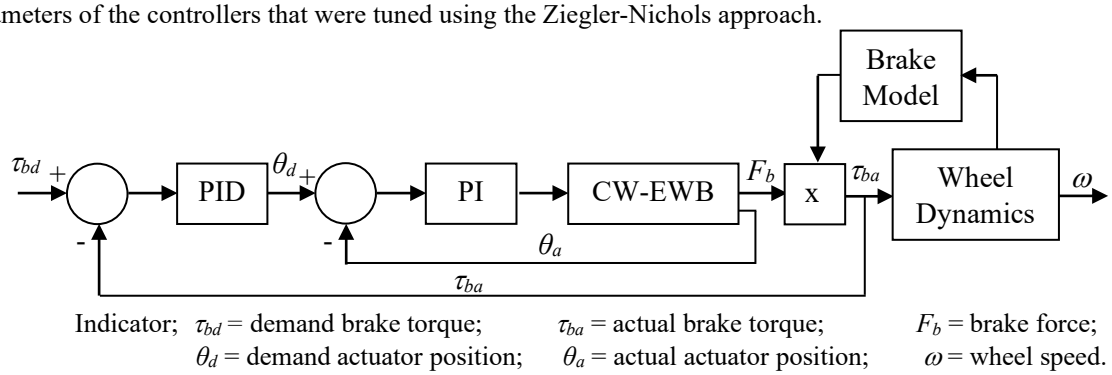

Figure 9. EWB torque control

Table 3. Controller parameters

Controller	k_P	k_I	k_D
Inner loop (Position)	0.000223	0.0005577	-
Outer loop (Torque)	0.0002087	0.00068318	1.435×10^{-5}

CW-EWB PROTOTYPE AND EXPERIMENTAL SETUP

Figure 10 shows the proposed CW-EWB hardware. The proposed CW-EWB is powered by a DC motor that is directly connected to the heart brake system, which consists of a wedge system, a calliper, and a brake pad, and uses a single lead screw style start. The lead screw, followed by a no-loss, is then connected to the heart mechanism to attain the expected actuation force. The lead screw converts the angular motion of the DC motor into the axial motion of the wedge in the middle of the brake. The EWB test rig, shown in Figure 11, is made up of an EWB actuator, a data acquisition device, a force sensor, a speed sensor, and an embedded encoder. The encoder detects rotational input to the calliper transmitted via the drive shaft. This input contains angular position and velocity values. The force sensor, which is linked to the brake calliper, determines the braking torque generated by the braking system, whereas the speed sensor determines the wheel speed. As the data logger, an NI PCI 6221 DAQ card outfitted with a National Instruments CB-68LP device was used for signal processing. The experiment was carried out using the hardware in the loops simulation (HILS) method, in which the vehicle model and CW-EWB controller run in simulation mode in the host PC while the real CW-EWB hardware serves as the brake actuator. The data logger connects the simulation and CW-EWB hardware via the Target PC. During experiments, the force sensor, speed sensor, and embedded encoder provide input signals to the CW-EWB controller and simulated vehicle via the data logger.

PERFORMANCE EVALUATIONS OF THE CW-EWB

The primary goal of this evaluation is to assess the validity of the proposed mathematical model of the CW-EWB and its control scheme, the capability of the braking system, and the potential utility of the proposed CW-EWB in giving a braking response to slow down a wheel. Because braking torque in the EWB can only be measured during dynamic braking, a sudden braking method test similar to that employed by [1,47,48] is applied in this work. This technique involves applying sufficient braking force to cause the load and wheel to slow down. Moreover, it attempts to simulate a critical braking situation in which the maximum performance of the braking system is adequately tested. In addition, the purpose of this test is to evaluate braking ability, which can play a crucial role in preventing accidents. In order to ensure the validity and compatibility of the mathematical model proposed for the CW-EWB, simulation and validation tests were performed with brake torque as the constant variable and wheel angular speed as the variable that was manipulated. Here, the desired braking torque was set to 730 Nm and 365 Nm at initial wheel speeds of 250 and 350 rpm, respectively.

The validation of the CW-EWB model employed actual system measurement techniques by comparing simulation results with experimental data utilising identical input signals. Model validation generally refers to establishing the degree to which the model and its accompanying data accurately match the actual vehicle system [4,35]. Despite the fact that the responses from the vehicle model do not necessarily match the simulated responses, confidence is gained that the model accurately simulates the EWB's behaviour. In addition, validation tests are used to determine if the input parameters for the vehicle model are reasonable and satisfy various simulation inputs. Some notations should be understood to facilitate comprehension of the result: the dotted lines represent the simulation command, the solid lines represent the simulation responses, and the dashed lines represent the experimental data.

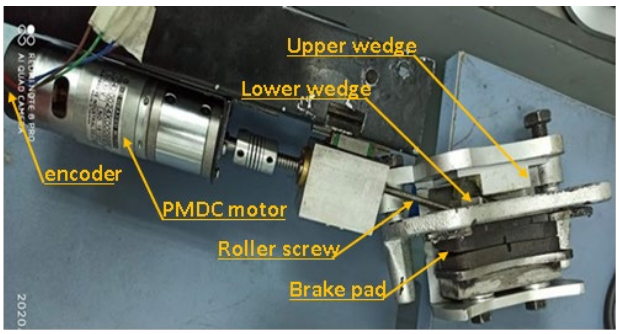

Figure 10. CW-EWB prototype

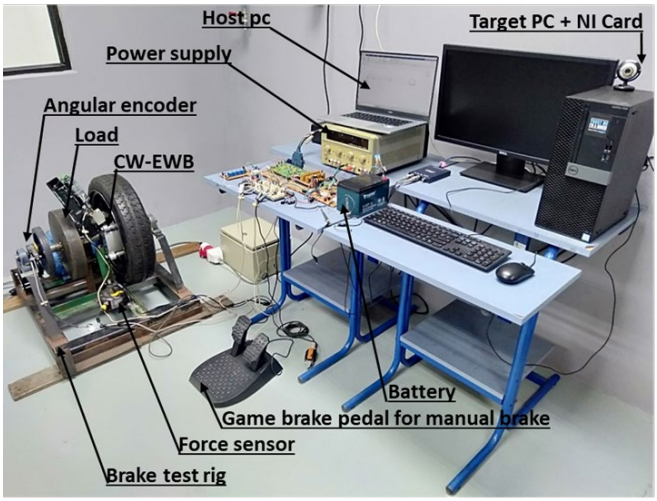

Figure 11. Brake test rig and experimental setup

Figures 12 to 15 show the simulation and experimental results. Figure 12(a) to 12(e) show the EWB brake torque, wedge position, voltage supply, current supply, and wheel speed, respectively. The braking torque command was applied at 2 seconds in all cases shown in Figures 12(a), 13(a), 14(a), and 15(a). In that condition, the EWB was already following the target torque in both simulation and experiment within the first two seconds. However, data incompatibility between the command and the simulation/experiment occurs most frequently during the transient phase, when the EWB was attempting to achieve the target torques. Response delays of up to 1 second and 1.23 seconds are produced by the simulation and experiment data, respectively. The difference in responses between the simulation/experimental result and the target was observed to be due to the actuator's inability to provide a quick response to the system.

In addition, it was observed that the issued command was a square input in which the step time was the same as the initial time, making it impossible for the simulation and hardware to trace the command. Even yet, if comparisons were conducted between the simulation and the experiment, the collected results indicate compatibility between them, where the simulation's trends exhibit a high degree of resemblance with the experiment, despite their magnitudes deviating somewhat in response. Noting that the differences between the simulation and the experimental data are fewer than 5%. Mechanical delay and internal frictions within the system's moving parts, which limit the system's relative speed, as well as a backlash at the connection between the DC motor and wedge mechanism, may account for experimental result variations.

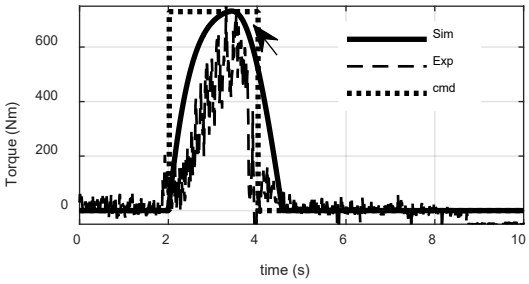

(a) brake torque produced by the EWB

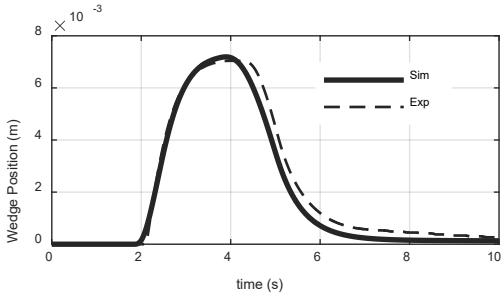

(b) wedge position

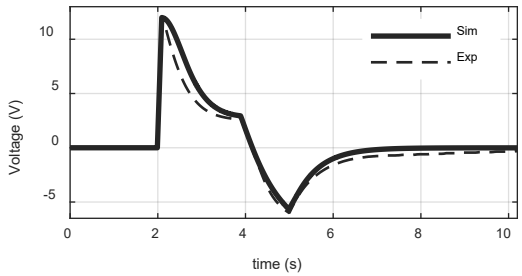

(c) voltage

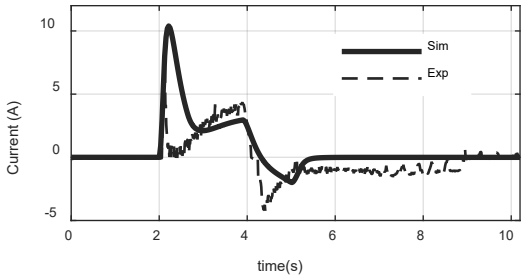

(d) current

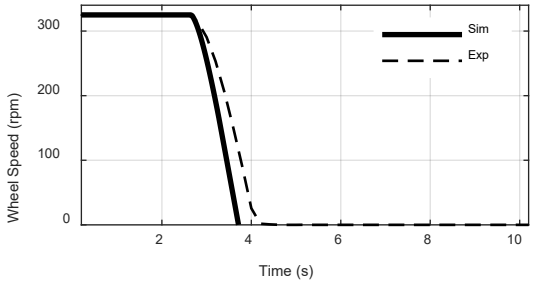

(e) wheel speed

Figure 12. Response of EWB with torque demand of 730 Nm at a wheel speed of 350 rpm

The results shown in graphs (a) of Figures 12 to 15 were also related to the wedge position response represented in graphs (b) of Figures 12 to 15. For the EWB to produce the desired torque, the upper wedge must relocate tangential to the brake rotor at some displacement from the initial conditions. Before conducting the experiments, the initial gap of the brake pad was set as close to the brake rotor as possible (approximately 0.002 m) using a filler gauge. As a result, when the brakes are applied, the brake pad remains engaged with the brake rotor, initiating the clamping mode. When the clamping force of the wedge mechanism applied to the brake rotor is sufficient, the kinetic energy of the rotating rotor will drag the brake pad along with the wedge mechanism, thereby producing a self-reinforcing force to slow the wheel speed. This condition often generates a sudden increase in brake torque, resulting in jerking phenomena at the first 2 to 2.3 seconds, as shown in the torque figures (a) (of Figures 12 to 15).

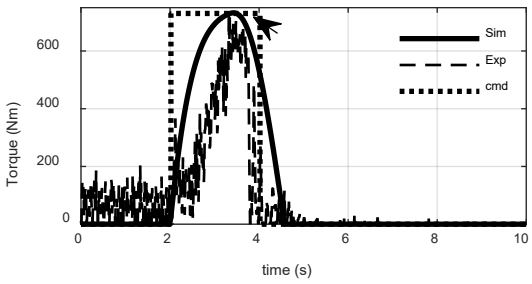

(a) Brake torque produce by the EWB

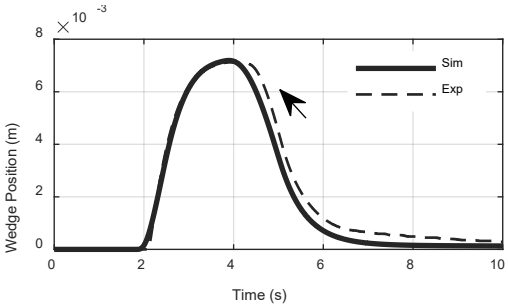

(b) Wedge position

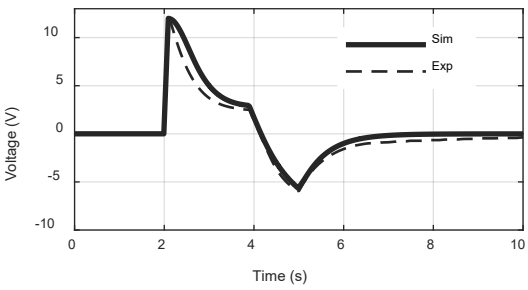

(c) Voltage

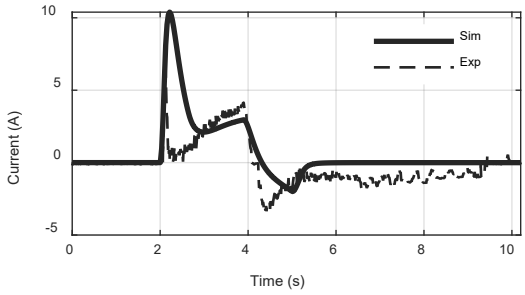

(d) Current

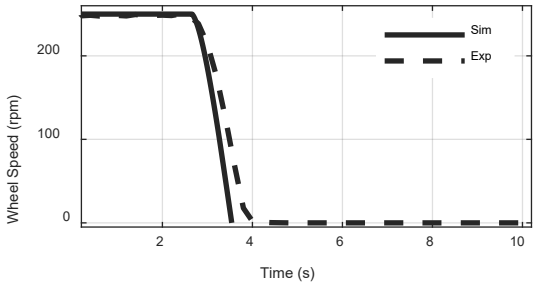

(e) wheel speed

Figure 13. Response of EWB with torque demand of 730 Nm at a wheel speed of 250 rpm

Furthermore, in terms of voltage usage, the responses of the EWB between simulation results and experimental data were nearly identical, falling within the 12 V range. As shown in graphs (c) of Figures 12 to 15, the simulation results closely match the response of the real EWB system with less than 5% error. On the other hand, these data reveal that the operation of the EWB requires only 12 V, which verifies prior studies [7,31,45,49,52]. Moreover, the performance of the EWB is tested by observing the behaviour of the drive motor current, as shown in graphs (d) of Figures 12 to 15. As shown in these figures, the trend between simulation and experimental data is nearly identical, with only a minor variance in magnitude. This circumstance happens when the internal resistance of the motor is not taken into account in the simulation model, causing the current value to be higher than the experiment. Furthermore, the motor parameters chosen may not coincide, resulting in disparities.

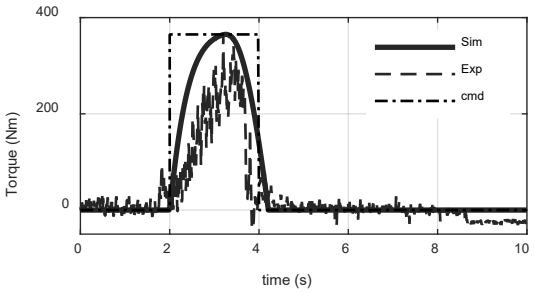

(a) brake torque produced by the EWB

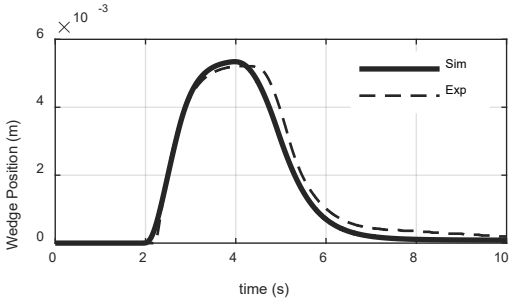

(b) wedge position

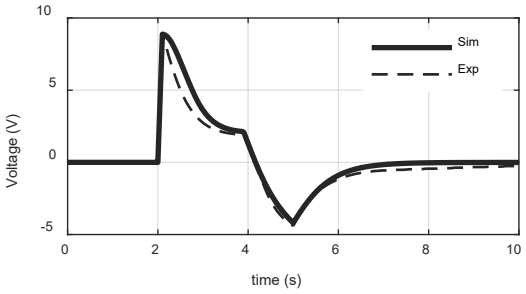

(c) voltage

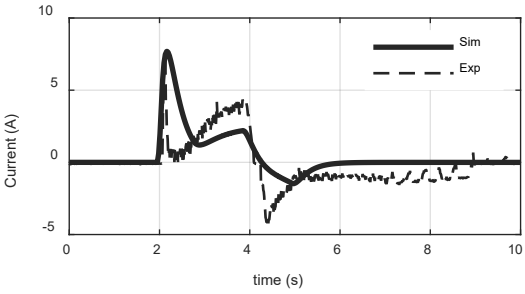

(d) current

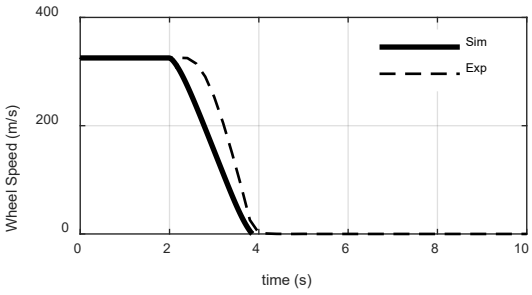

(e) wheel speed

Figure 14. Response of EWB with torque demand of 365 Nm at a wheel speed of 350 rpm

The braking test conducted in this study showed that the suggested EWB system functioned successfully, as evidenced by its potential to be used in a vehicle braking application. Graphs (e) from Figures 12–15 indicate that the EWB can deliver the necessary braking torque to slow down the wheel speed in both simulation and real-world systems. There are

some differences between the experimental and simulation responses, with the experimental responses being up to 0.5 seconds slower than the simulation responses. These differences are typically caused by internal frictions within the hardware system, particularly between two rough contact surfaces, as well as the inertia of the internal component of the DC motor, which causes the experiment's slow response, as previously discussed.

According to Ahmad [4], the trend of the model response is the most important characteristic of a control-oriented model. As long as the trend of the model responses closely resembles the trend of the measured responses, with acceptable deviations and errors, the results are appropriate. In addition, Rykiel et al. [50] stated that the acceptable level of deviation between measured and simulated responses should be less than 5%. According to Ahmad et al. [3], the maximum acceptable error for conveying the credibility of a simulation is 5%. On the other hand, numerous scholars, like Ahmad [4] and Oreskes et al. [51], have claimed that the permissible time delay between simulation and experiment is less than one second. As a result of these statements, it is possible to conclude that the model is realistic and acceptable for future development.

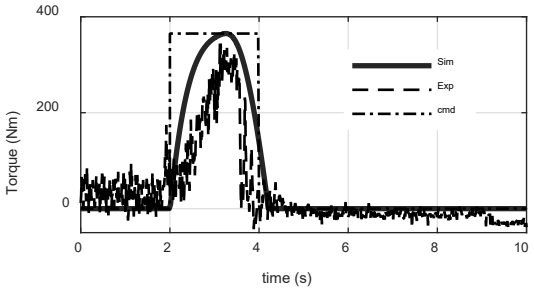

(a) brake torque produced by the EWB

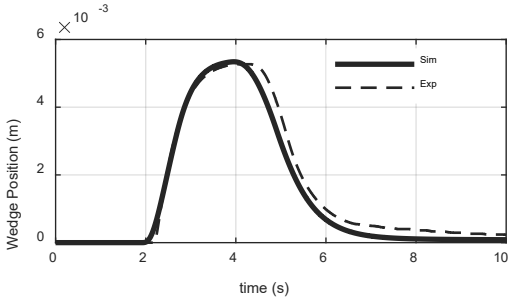

(b) wedge position

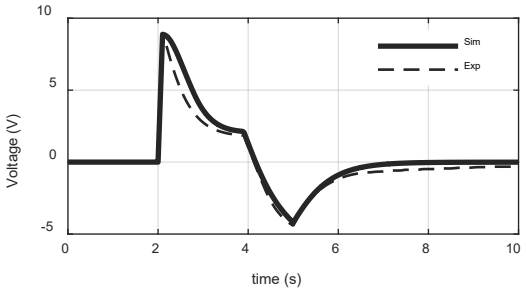

(c) voltage

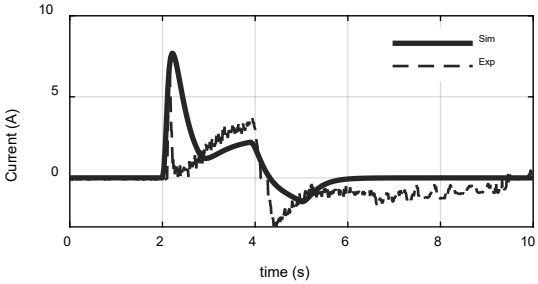

(d) current

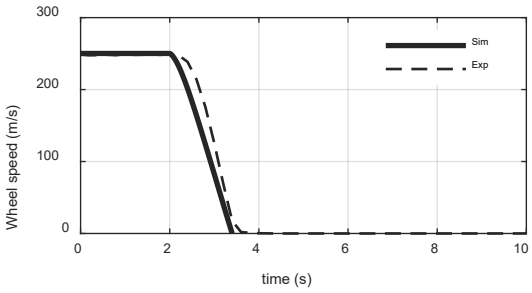

(e) wheel speed

Figure 15. Response of EWB with torque demand of 365 Nm at a wheel speed of 250 rpm

CONCLUSIONS

In this study, a new EWB called the CW-EWB was designed and built. The CW-EWB system is made up of a wedge mechanism, a lead screw, a brake pad, and an electric motor that serves as the actuator. The kinematic and dynamic mode models of the brake mechanism were built to characterise the dynamic behaviour of the proposed CW-EWB. The brake torque produced by the CW-EWB system can therefore be determined by integrating the CW-EWB model with the brake torque model in the contact interface. A brake torque control-based PID controller was created utilising the derived CW-EWB model. The controller approach comprised of two control loops; position control loop and brake torque control loop. Torque tracking control of the CW-EWB was done in both simulation and experimental studies to validate the effectiveness of the suggested controller technique as well as the simulation model. Several tests were carried out, including brake torque demands of 730 and 365 Nm at speeds of 350 and 250 rpm, respectively. In comparison to its benchmark, the results showed that the proposed CW-EWB model and an appropriate control structure were able to make good performance and closely track the preferred torques. In addition, it was observed that the proposed control structure

could track the brake command with acceptable errors and deviations. The torque control scheme is thus appropriate for application in the inner loop of the passive braking system as well as the ABS system in future research.

ACKNOWLEDGEMENT

The authors would like to express their gratitude to UTeM for funding this research through an internal grant PJP/2020/FKM/PP/S01783 lead by Ir. Dr. Ts. Fauzi Ahmad.

DECLARATION OF CONFLICTING INTEREST

The authors declare that there is no conflict of interest.

REFERENCES

[1] F. Ahmad, K. Hudha, S. A. Mazlan, H. Jamaluddin, V. R. Aparow, and M. R. M. Yunos, "Simulation and experimental investigation of vehicle braking system employing a fixed caliper based electronic wedge brake," *Simulation*, vol. 94, no. 4, pp. 327–340, 2018.

[2] Z. Zhu, X. Wang, J. Yan, L. Li, and Q. Wu, "A dynamic decoupling control method for PMSM of brake-by-wire system based on parameters estimation," *IEEE/ASME Transactions on Mechatronics*, vol. 27, no. 5, pp. 3762–3772, 2022.

[3] Ahmad F, Hudha K, Mazlan SA, Jamaluddin H, Zamzuri H, Kadir ZA, et al., "Modelling and control of a fixed calliper-based electronic wedge brake," *Strojniški vestnik – Journal of Mechanical Engineering,* vol. 63, no. 3, pp. 181–190, 2017.

[4] F. Ahmad, "Adaptive fuzzy fractional proportional integral derivative controller for antilock braking system using electronic wedge brake," Ph.D thesis, Universiti Teknologi Malaysia, Malaysia 2018.

[5] F. Ahmad, S. A. Mazlan, H. Zamzuri, K. Hudha, and H. Jamaluddin, "Study on the potential application of electronic wedge brake for vehicle brake system," *International Journal of Modelling, Identification and Control*, vol. 23, no. 4, p. 306, 2015.

[6] H. Hartmann, M. Schautt, A. Pascucci, and B. Gombert, "eBrake ® – The Mechatronic Wedge Brake," *SAE Technical Papers*, pp. 2002-01–2582, 2002.

[7] Roberts R, Gombert B, Hartmann H, Lange D, Schautt M, Hartmann H, et al., "Testing the mechatronic wedge brake," *SAE Technical Papers*, vol. 1, no. 724, pp. 2004-01–2766, 2004.

[8] L. M. Ho, R. Roberts, H. Hartmann, and B. Gombert, "The electronic wedge brake-EWB*," SAE Technical Papers*, no. 2006-01-3196, 2006.

[9] H. S. Kim, C. H. Jo, S. M. Lee, and H. Lim, "Electronic wedge brake system," US 2010/0140028A1, 2010.

[10] J.G. Kim, M.J. Kim, J.K. Kim, K.H. Noh, "Developing of electronic wedge brake with cross wedge," *SAE Technical Papers*, pp. 2009-01–0856, 2009.

[11] P. Dongri, "Single motor electronic control wedge type brake system," CN101328941B, 2011.

[12] G. Jaeseung Cheon, "Single motor electronic wedge brake system locking parking force," US 2009/0071769 A1, 2009.

[13] D. Park, "Single motor electronic controlled wedge brake system," US 8151947 B2, 2012.

[14] Jīnzhōngchéng, "Single motor electro wedge brake system using solenoid mechanism for implementing additional functions," CN101332812 A, 2008.

[15] L. Jinlong, "Electronic wedge brake system," CN202703552 U, 2013.

[16] L. Jinlong, "Electronic wedge drum brake," CN202707879 U, 2013.

[17] J. Kim, "Electronic wedge brake apparatus," US 8733514 B2, 2014.

[18] A. Ghajari and R. Kazemi, "A new approach to the electronic wedge brake," *SAE Technical Papers*, no. 2012–01–1801, 2012.

[19] C.H. Jo, S.M. Lee, H.L. Song, Y.S. Cho, I. Kim, D.Y. Hyun, et al., "Design and control of an upper-wedge-type electronic brake," *Proceedings of the Institution of Mechanical Engineers, Part D: Journal of Automobile Engineering*, vol. 224, no. 11, pp. 1393–1405, 2010.

[20] M. L. H. A. Rahman, K. Hudha, F. Ahmad, and H. Jamaluddin, "Design and clamping force modelling of electronic wedge brake system for automotive application," *International Journal of Vehicle Systems Modelling and Testing*, vol. 8, no. 2, p. 145, 2013.

[21] D. H. Shin and J. N. An, "Study of stiffness design of caliper for reducing the weight of an electro wedge brake," *Applied Mechanics and Materials*, vol. 138–139, pp. 159–162, 2012.

[22] Á. Semsey and R. Roberts, "Simulation in the development of the electronic wedge brake," *SAE Technical Papers*, vol. 1, no. 724, 2006.

[23] M. A. A. Emam, A. S. Emam, S. M. El-Demerdash, S. M. Shaban, and M. A. Mahmoud, "Performance of automotive self reinforcement brake system," *Journal of Mechanical Engineering,* vol. 1, no. 1, pp. 4–10, 2012.

[24] H. Yongping, Y. Junbo, and S. Weiping, "A kind of electronic wedge brake," CN105570350B, 2015.

[25] Fu Yunfeng, "A kind of automotive electronics wedge brake," CN109356950A, 2019.

[26] Y. Ming, C. Hongjie, M. Jiayu, W. Pengjing, and C. Shi'an, "Electronic wedge type braking device based on electric pole direct drive and braking method thereof," CN109606337B, 2021.

[27] I. Kim, "Method for controlling braking of vehicle," US8903621B2, 2014.

[28] M. S. Jneid and A. Joukhadar, "LQR-based control of a single motor electronic wedge brake EWB for automotive brake-by-wire system," *Soft Computing Electrical Engineering*, vol. 1, no. 1, pp. 12–35, 2019.

[29] H. M. Abdel-Rahman, A. O. Moaaz, N. M. Ghazaly, and A. M. A. El Tawwab, "Investigation of a new wedge disc brake mechanism," *International Journal of Mechanical and Production Engineering Research and Development,* vol. 9, no. 6, pp. 585–594, 2019.

[30] M. Yao, J. Miao, S. Cao, S. Chen, and H. Chai, "The structure design and optimisation of electromagnetic-mechanical wedge brake system," *IEEE Access*, vol. 8, pp. 3996–4004, 2020.

[31] S. I. Haris, M. H. C. Hassan, F. Ahmad, and A. K. M. Yamin, "Performance evaluation of vehicle braking system employing an electronic wedge brake mechanism," *Proceedings of the 7th International Conference and Exhibition on Sustainable Energy and Advanced Materials (ICE-SEAM 2021)*, Melaka, Malaysia, pp. 269–273, 2021.
[32] S. I. Haris, F. Ahmad, M. H. C. Hassan, A. K. M. Yamin, and N. R. M. Nuri, "Self tuning PID control of antilock braking system using electronic wedge brake," *International Journal of Automotive and Mechanical Engineering*, vol. 18, no. 4, pp. 9333–9348, 2021.
[33] E. Arasteh and F. Assadian, "A comparative analysis of brake-by-wire smart actuators using optimisation strategies," *Energies*, vol. 15, no. 2, 2022.
[34] F. Xu and C. Cho, "A novel electronic wedge brake based on active disturbance rejection control," *Energies*, vol. 15, no. 14, pp. 1–18, 2022.
[35] S. I. Haris, F. Ahmad, M. H. C. Hasan, and A. K. M. Yamin, "Experimental evaluation of cone wedge shape based electronic wedge brake mechanism in vehicle braking system," *Automotive Experiences*, vol. 5, no. 3, pp. 433–451, 2022.
[36] J. Kim, "Single motor electro wedge brake system using solenoid mechanism for implementing additional functions," US 7987950 B2, 2011.
[37] Q. Liu, L. Chen, and J. Chen, "Analytical study on dynamics of wedge braking systems with time delay," presented at INTER-NOISE 2019 MADRID - 48th International Congress and Exposition on Noise Control Engineering, Madrid, Spain, 2019.
[38] M. Soomro, M. K. Hassan, and F. Ahmad, "Modelling and validation of an electronic wedge brake system with realistic Quarter Car Model for anti-lock braking system design," *International Journal of Integrated Engineering*, vol. 11, no. 4, pp. 70–80, 2019.
[39] E. Arasteh and F. Assadian, "Bond graph modeling of brake-by-wire actuators on a one-wheel vehicle model," *Society for Modeling and Simulation International,* vol. 53, no. 3, pp. 169–178, 2021.
[40] SAE International Vehicle Recommended Practice, "Friction coefficient identification and environmental marking system for brake lining," 2012.
[41] Gombert B, Ho LM, Roberts R, Fox J, Baier-Welt C, Lacraru L, et al. "Modeling and control of a single motor electronic wedge brake," *SAE Technical Papers Series*, vol. 1, no. 724, pp. 2007-01–0866, 2010.
[42] M. H. Che Hasan, M. K. Hassan, F. Ahmad, M. H. Marhaban, and S. I. Haris, "A dynamic model of electronic wedge brake: Experimental, control and optimisation," *Indonesian Journal of Electrical Engineering and Computer Science*, vol. 23, no. 2, pp. 740–751, 2021.
[43] K. Han, K. Huh, J. Chun, M. Kim, and J. Kim, "Design of hardware architecture and control algorithm for the electronic wedge brake," *Proceedings of the ASME 2010 Dynamic Systems & Control Conference*, vol. 44182, pp. 821–826, 2010.
[44] K. Han, M. Kim, and K. Huh, "Modeling and control of an electronic wedge brake," *Proceedings of the Institution of Mechanical Engineers, Part C: Journal of Mechanical Engineering Science*, vol. 226, no. 10, pp. 2440–2455, 2012.
[45] M. H. Che Hasan, M. Khair Hassan, F. Ahmad, and M. H. Marhaban, "Modelling and design of optimised electronic wedge brake," *IEEE International Conference on. Automatic Control and Intelligent Systems,* no. June, pp. 189–193, 2019
[46] M. H. Che Hasan, M. K. Hassan, F. Ahmad, and M. H. Marhaban, "Electronic wedge brake model approximation analysis," *Proceedings of Mechanical Engineering Research Day 2020*, no. December, pp. 26–27, 2020.
[47] A.Z. Zainordin, Z. Mohamed, and F. Ahmad, "Magnetorheological fluid: testing on automotive braking system," *International Journal of Automotive and Mechanical Engineering*, vol. 18, no. 1, pp. 8577–8584, 2021.
[48] M. Shukri, A. Razak, F. Ahmad, and M. A. Abdullah, "Simulation of adaptive cruise control for autonomous vehicle using throttle by wire and electronic wedge brake," *Proceedings of Malaysian Technical Universities Conference on Engineering and Technology (MUCET) 2021*, no. 1, pp. 118–119, 2021.
[49] J. G. Kim, M. J. Kim, J. H. Chun, and K. Huh, "ABS / ESC / EPB control of electronic wedge brake," *SAE Technical Papers*, no. 2010-01–0074, 2012.
[50] E.J. Rykiel, "Testing ecological models: The meaning of validation," *Ecological Modelling*, vol. 90, no. 3, pp. 229–244, 1996.
[51] Oreskes N, Shrader-Frechette K, Belitz K. Verification, validation, and confirmation of numerical models in the earth sciences. *Science (80).* vol. 263, no. 5147, pp. 641–6, 1994.
[52] M. H. Che Hasan, M. K. Hassan, F. Ahmad, and S. I. Haris, "Analytical versus optimisation PID tuning for electronic wedge brake clamping force control," *Proceedings of Malaysian Technical Universities Conference on Engineering and Technology (MUCET) 2021*, pp. 110–111, 2021.